

See discussions, stats, and author profiles for this publication at: <https://www.researchgate.net/publication/333939982>

Solution Processable Deep-Red Phosphorescent Pt(II) Complex: Direct Conversion from Its Pt(IV) Species via a Base Promoted Reduction

Article in *ACS Applied Electronic Materials* · June 2019

DOI: 10.1021/acsaem.9b00246

CITATIONS

10

READS

161

17 authors, including:



Hyunsoo Lim

The University of Queensland

36 PUBLICATIONS 1,160 CITATIONS

[SEE PROFILE](#)



Atul Shukla

The University of Queensland

35 PUBLICATIONS 330 CITATIONS

[SEE PROFILE](#)



Viqar Ahmad

The University of Queensland

14 PUBLICATIONS 110 CITATIONS

[SEE PROFILE](#)



Monirul Hasan

The University of Queensland

24 PUBLICATIONS 104 CITATIONS

[SEE PROFILE](#)

Some of the authors of this publication are also working on these related projects:



High Efficiency Hybrid/ Organic Light-Emitting Devices [View project](#)



Organic Electronic Devices [View project](#)

Solution Processable Deep-Red Phosphorescent Pt(II) Complex: Direct Conversion from Its Pt(IV) Species via a Base-Promoted Reduction

Ilene Allison,^{†,‡,§} Hyunsoo Lim,^{†,§} Atul Shukla,^{†,§} Viqar Ahmad,^{†,§} Monirul Hasan,^{†,§} Kedar Deshmukh,^{†,§} Robert Wawrzinek,^{†,§} Sarah K. M. McGregor,^{†,‡,§} Jack K. Clegg,^{‡,§} Velayudhan V. Divya,^{||} Chinju Govind,^{||} Cherumuttathu H. Suresh,^{||} Venugopal Karunakaran,^{||} Narayanan Unni K. N.,^{||} Ayyappanpillai Ajayaghosh,^{||} Ebinazar B. Namdas,^{*,†,§} and Shih-Chun Lo^{*,†,‡,§}

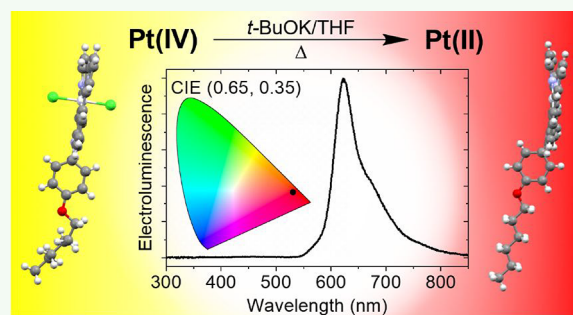
[†]Centre for Organic Photonics & Electronics, [‡]School of Chemistry and Molecular Biosciences, and [§]School of Mathematics and Physics, The University of Queensland, Brisbane, QLD 4072, Australia

^{||}Photosciences and Photonics Section, Chemical Sciences and Technology Division, CSIR-National Institute for Interdisciplinary Science and Technology, Trivandrum 695019, India

Supporting Information

ABSTRACT: Color purity is a critical prerequisite for full color displays. Creation of deep-red phosphorescent materials with high PLQYs is particularly challenging because of the “energy gap law”. Simultaneously achieving high yielding solution processable Pt(II) complexes further complicates this challenge. In this report, we developed a high-yielding synthetic route to a solution processable/deep-red Pt(II) complex with a rigid tetradentate structure, in which we identified an octahedral Pt(IV) complex as a major side product formed under the standard complexation conditions. We managed to effectively transform the octahedral Pt(IV) species into a highly luminescent deep-red square-planar Pt(II) complex through a base-promoted reduction. The Pt(II) complex was found to exhibit high solution and blend film PLQYs. X-ray crystal structure and DFT calculations of the Pt(II) complex showed that perpendicular orientation of molecular dipoles enhanced the luminescence properties. In neat films, there was no luminescence enhancement due to interdigitation of the attached hexyloxy tails, preventing strong Pt···Pt interactions in the solid state. Solution-processed OLEDs based on the Pt(II) complex showed a low turn-on voltage of 3.3 V (at 1 cd/m²) with a maximum brightness of 2000 cd/m² and a maximum EQE of ≈6% (4% at 100 cd/m²). A narrow electroluminescence with a full width at half-maximum of ≈50 nm was observed with a peak at 623 nm and deep-red emission with 1931 CIE coordinates of (0.65, 0.35). Transient electroluminescence measurements were used to investigate the EQE roll-off of the OLEDs.

KEYWORDS: deep-red phosphorescence, solution processed, OLEDs, rigid tetradentate, platinum complex, base-promoted reduction



INTRODUCTION

Organic light-emitting diodes (OLEDs) have retained research attention due to several characteristic features including their ability to emit efficiently with fast response times, the tunability of desirable properties, mechanical flexibility, and the ability to incorporate them into devices by using fast, low-temperature, and cheaper solution-processing methods. These advantages have facilitated commercialization of high-end OLED products such as full color displays for televisions and mobile phones as well as solid-state lighting.^{1,2}

While many factors contribute to OLED performance, there is a large dependence on the type of material used. In accordance with spin statistics, conventional fluorescent emitters tend to have low device external quantum efficiency (EQE) as electroluminescence (EL) is limited to singlet

excitons, which only represent 25% of all excitons generated in the device. The other 75% of excitons are generated as triplets, which do not emit light as it is a spin-forbidden process.³ Device EQEs can be increased by harnessing the otherwise lost triplet excitons, using phosphorescent materials or, more recently, materials that exhibit thermally activated delayed fluorescence (TADF).⁴ Phosphorescent transition metal complexes achieve triplet harvesting through strong spin-orbit coupling, which facilitates effective intersystem crossing. Highly efficient phosphorescent OLEDs have been demonstrated by using Ir(III), Os(II), and Pt(II) complexes.^{5–12}

Received: April 22, 2019

Accepted: June 21, 2019

Published: June 21, 2019

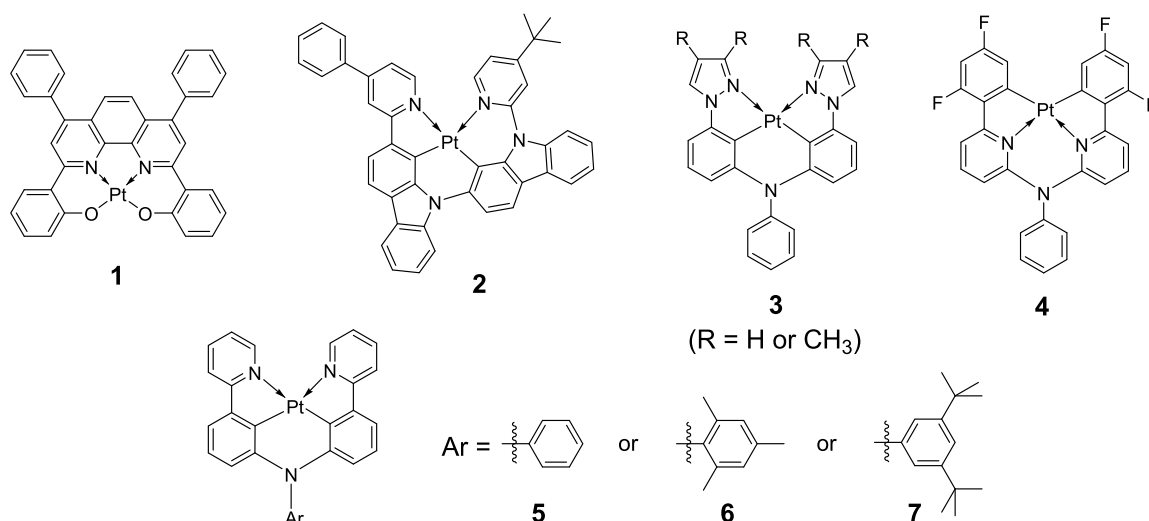
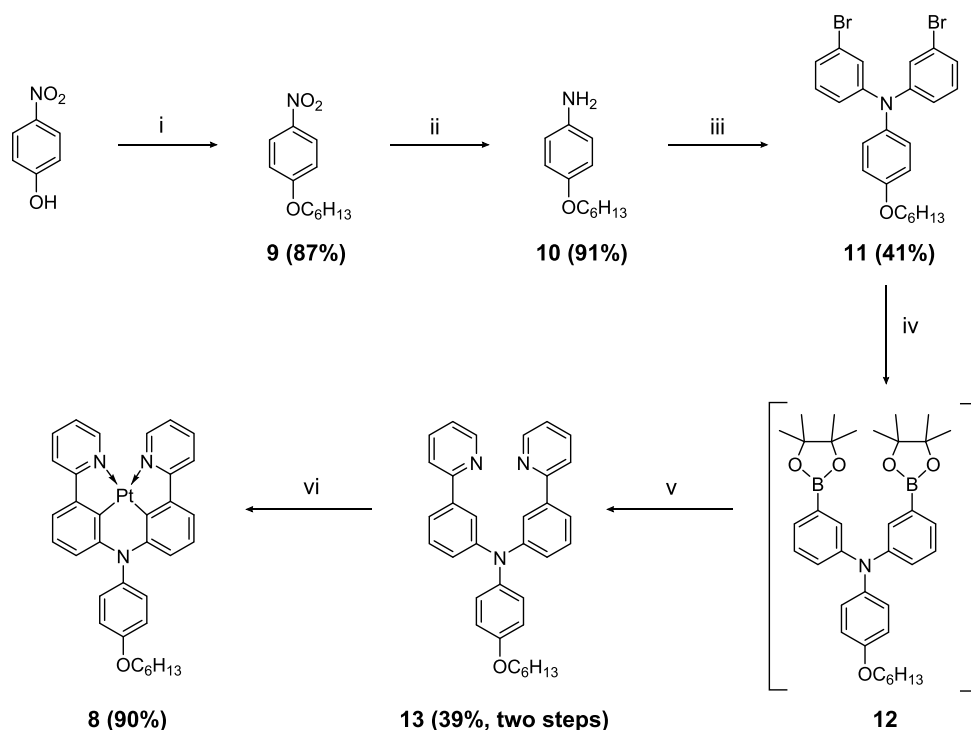


Figure 1. Examples of rigid multidentate cyclometalated Pt(II) complexes.^{29–33}

Scheme 1. Synthetic Route to Pt(II) Complex 8^a



^aReagents and conditions: (i) K₂CO₃, 1-bromohexane, acetone, heat, Ar_(g); (ii) 10% Pt/C, H₂, EtOAc, MeOH, RT, Ar_(g); (iii) CuI, *t*-BuOK, 1,10-phenanthroline, 1-bromo-3-iodobenzene, xylene, heat, Ar_(g); (iv) *n*-BuLi, 2-isopropoxy-4,4,5,5-tetramethyl-1,3,2-dioxaborolane, THF, –78 °C to RT, Ar_(g); (v) 2-bromopyridine, 2 M Na₂CO_{3(aq)}, Pd(PPh₃)₄, toluene, EtOH, heat, Ar_(g); (vi) (a) PtCl₂, benzonitrile, heat, Ar_(g), (b) *t*-BuOK, THF, heat, Ar_(g).

Color purity is critical for full color displays, where highly efficient deep-blue, green, and red phosphorescent emitters are required. Phosphorescent materials with deep-red emission are challenging to develop as they generally suffer from low photoluminescence quantum yields (PLQYs) due to the “energy gap law”.^{13–18} This law describes the strong coupling of ground and excited states by vibronic overlap. Consequently, nonradiative decay rates (k_{nr}) are exceptionally high, ultimately decreasing PLQYs. Nevertheless, a number of octahedral Ir(III) complexes have been reported to show efficient solution-processed OLEDs with CIE coordinates that

match commercial red emitters (CIE ≈ 0.65, 0.35).¹⁹ These complexes include [Ir(Th-PQ)₃], TPQIr-ET, and Ir(DPA-Fly-CF₃)₂acac, and the associated OLEDs showed excellent maximum EQEs of 17–21%.^{20–22} Comparatively, square-planar Pt(II) complexes have been much less studied even though they provide unique properties beneficial to red phosphorescent OLEDs and organic light-emitting field-effect transistors (OLETs).^{23–25}

A plausible strategy to counteract the “energy gap law” is to suppress k_{nr} . For example, by limiting geometric reorganization between the ground and excited states, rigid multidentate

cyclometalated Pt(II) motifs have been shown to achieve this. Furthermore, rigid tetradentate chelates offer enhanced chemical and physical stability, thereby significantly increasing the device lifetime.^{23,26–28} Although rigid Pt(II) complexes offer moderate to high PLQYs with impressive OLED device performance (Figure 1), efforts toward synthesis of Pt(II) complexes (both rigid and nonrigid) have, in general, suffered from low to moderate yields.^{26,29–33} There has been no report on the origin responsible for the low reaction yields which deters their advancement and potential use. More importantly, a subsection of these gave efficient deep-red OLEDs, but were exclusively fabricated by vacuum deposition,^{31–34} rendering them unsuitable for fast, low-temperature, and low-cost device manufacturing methods such as spin-coating or inkjet printing.

To the best of our knowledge, no solution processable deep-red Pt(II) complexes exploiting the aforementioned strategy have been reported. There have, however, been reports of solution processable Pt(II) complexes with orange-red emission peaks at ≈ 580 nm with good EQEs of about 3–10%.^{35–37}

In addition, square-planar Pt(II) chromophores can potentially show efficient π - π stacking and strong Pt...Pt interactions at their vacant axial sites, which in turn promote molecular aggregates or excimers in solid state. These aggregates, instead of suffering from typical aggregation caused quenching (ACQ) of luminescence, exhibit an enhancement through long-range order facilitated by a unique metal-metal-to-ligand charge transfer (MMLCT) process.^{38–40} The MMLCT transition also features a bathochromic shift and featureless emission spectrum. MMLCT has given rise to a high neat film PLQY (up to 96%) and a comparatively short emission lifetime (<400 ns).⁴¹ An extremely high EQE of >45% has been theoretically predicted if the transition dipole moments of the complexes can be horizontally aligned to the device substrate, leading to a high light outcoupling efficiency without the aid of any refractive index structures. Recently, by exploiting these aggregate phenomena and the orientation of emitting dipoles, Kim et al. demonstrated a vacuum-deposited Pt(fppz)₂ device with a record EQE of $\approx 39\%$ and an EL peak at ≈ 620 nm.⁴¹

In this article, we report the synthesis, photophysical properties, and electroluminescent studies of a solution processable deep-red Pt(II) complex **8** (Scheme 1) with a rigid structural motif. In the key step of material synthesis, we isolated a major octahedral Pt(IV) side product formed in standard complexation conditions along with a trace amount of the desired square-planar Pt(II) complex. We found the side product can be readily converted into a luminescent deep-red Pt(II) complex under a base-promoted reduction. Compared to its parent Pt(II) complex **5**, the attachment of a hexyloxy solubilizing moiety to the aminophenyl bridge not only enables solution processability but also leads to a high solution and blend-film PLQYs ($50 \pm 3\%$ and $55 \pm 4\%$, respectively). Solution-processed OLEDs based on **8** showed a low turn-on voltage of 3.3 V (at 1 cd/m²) with a maximum EQE of 6.1% (4% at 100 cd/m²) and a maximum brightness of 2000 cd/m². The electroluminescence is narrow with a fwhm of ≈ 50 nm and a peak at 623 nm, giving rise to a deep-red emission with CIE coordinates of (0.65, 0.35). DFT calculations, transient photoluminescence, and transient electroluminescence were conducted to gain insights into its photophysical processes, including exciton generation and recombination.

RESULTS AND DISCUSSION

Synthesis. The synthesis of the solution processable Pt(II) complex **8** was accomplished by using a linear synthetic approach as outlined in Scheme 1. First, a solubilizing *n*-hexyl group was attached to nitrophenol via a Williamson ether synthesis to give **9** in a good yield (87%). Subsequently, the nitro functional group was reduced to the respective amine **10** in an excellent yield of 97% under Pt/C-catalyzed hydro-generation conditions, although we found that the reduction of **9** could also be accomplished with other metals such as Pd and Fe in good yields (80–83%).⁴² To produce the tetradentate ligand precursor **11**, we made use of an economical copper-catalyzed Ullmann coupling reaction with an excess of 1-bromo-3-iodobenzene.⁴³ The synthesis was followed by a double borylation of **11** with 2-isopropoxy-4,4,5,5-tetramethyl-1,3,2-dioxaborolane and then a double-palladium-catalyzed Suzuki cross-coupling with 2-bromopyridine. This gave ligand **13** in a 39% yield over the two steps (diborylations and di-Suzuki cross-couplings). Finally, the target Pt(II) complex **8** was successfully produced by a one-pot process in an excellent overall yield of 90%. First, our cyclometalation of PtCl₂ with **13** was conducted in dilute benzonitrile (≈ 0.02 M) to avoid the undesired formation of oligomers or polymers.³⁰ This indeed generated the desired Pt(II) complex **8** in a trace amount; see Figure S3c in the Supporting Information for the crude ¹H NMR spectrum, dominated by a yellow Pt(IV) complex analogous to **8**, except for the addition of two axial chlorido ligands (see the mass spectrum in Figure S4, crystallography in Figure S5, and ¹H NMR spectra in Figure S3c). While the real mechanism in forming the *trans*-octahedral Pt(IV) complex remains unclear, oxidation of the metal likely results from the low ionization potential of **8** (see the Thermal and Electrochemical Properties section) in the presence of the electron-deficient benzonitrile solvent. In fact, similar oxidation of Pt(II) to Pt(IV) complexes has only been investigated through either thermal or photochemical processes⁴⁴ with dihalogens (I₂ and Br₂),⁴⁵ alkyl halides,⁴⁶ iodobenzene dichloride,^{47–50} or peroxides⁵¹ to predominantly give octahedral Pt(IV) species with the two chlorido ligands *cis* to each other. Direct one-pot formation of Pt(IV) complexes from cyclometallic ligands with Pt(II) precursors is, however, more scarce and has only been shown recently, where Bruce et al.⁵² and Su et al.⁵³ reported respective *cis*- and *trans*-octahedral Pt(IV) complexes, using a similar Pt(II) precursor, K₂PtCl₄. This might have explained the low to moderate yields in most attempts to isolate the square-planar Pt(II) complexes.^{30–32,34,37,54–58} Remarkably, we found that the *trans*-octahedral Pt(IV) complex could be readily converted into its square-planar Pt(II) complex **8** in an excellent yield of 90% by treating the crude reaction mixture that contained the Pt(IV) and Pt(II) complexes with a base such as potassium *tert*-butoxide (*t*-BuOK) in tetrahydrofuran (THF) at reflux (Figure S3a,b). Interestingly, a similar base-promoted reduction of Pt(IV) complexes, bearing with *trans* dichlorido coligands, into Pt(II) derivatives was found in non-cyclometallic Pt(IV) complexes.⁵⁹ Finally, it is worth noting that to isolate **8**, we used a triethylamine deactivated silica column chromatography as **8** was found prone to degradation on nontreated silica (and also in chloroform) due to the electron richness of the bridging amine, making the complex prone to protonation.

Structural Properties. X-ray crystallography was pursued to verify the chemical structure of **8**, where the single crystals

were grown from liquid–liquid diffusion of light petroleum and dichloromethane. The X-ray crystal structure (Figure 2a)

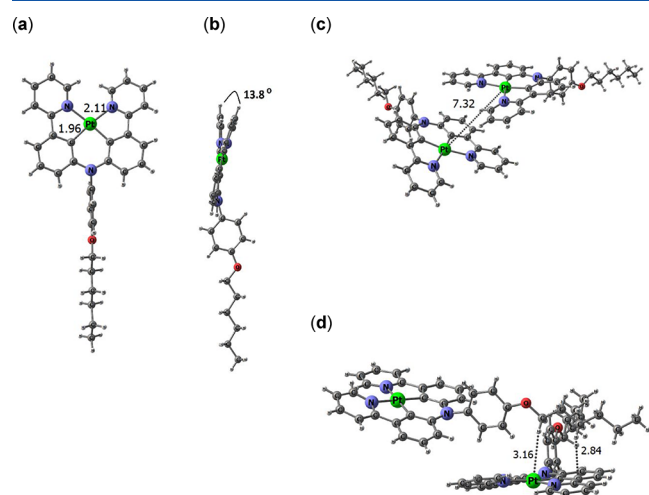


Figure 2. X-ray crystal structure of **8**. (a) Top view. (b) Side view. (c) A dimer unit (**8**...**8**)-a in a distorted π -stacking arrangement. (d) A dimer unit (**8**...**8**)-b, showing alkyl chain interaction with the metal center. All distances in Å.

showed a slightly distorted square-planar geometry with a distortion angle (θ) of 13.8° (Figure 2b), which can be attributed to steric repulsion of the two pyridyl hydrogens (α to the nitrogen) on the two adjacent ligands. Interestingly, the distortion still occurred despite the Pt–N bond lengths (2.11 Å) being slightly longer than the Pt–C bond lengths (1.96 Å), meaning that the pyridyl rings are further apart from one another than the phenyl rings. The shortest Pt...Pt distance in the packing was found to be 7.32 Å in a dimer unit (**8**...**8**)-a (Figure 2c), where the monomers are arranged in a distorted π -stacking manner. The C...C distance observed in (**8**...**8**)-a was 3.25 Å, indicating π – π interactions between the pyridyl and phenyl moieties while the CH...N distance was 2.85 Å, indicating CH– π interaction between the two pyridyl moieties. Another dimer unit (**8**...**8**)-b (Figure 2d) showed strong alkyl interactions arising from interdigitation of the hexyloxy tails of one monomer with another, where the CH...Pt interaction distances of 3.16 Å and other CH– π interactions protect the Pt center from direct Pt...Pt interactions. The crystal is also rich with CH– π interactions due to the nearly perpendicular orientation of one monomer to another, providing an edge-to-face herringbone packing motif (Figure S6). The interdigitation of the hexyloxy tails in **8** prevents strong Pt...Pt interaction, limiting the possibility of MMLCT.^{38–40}

Thermal and Electrochemical Properties. Thermal properties of Pt(II) complex **8** were studied by using thermogravimetric analysis (TGA) and differential scanning calorimetry (DSC). **8** was found to exhibit high thermal stability with 5% weight loss at about 370°C (Figure S7). No detectable glass transition temperature was found for **8** in DSC with a measured range of -50 to 250°C (Figure S8).

Electrochemical properties of **8** were probed by using cyclic voltammetry (CV). While redox processes of square-planar Pt(II) complexes are often reported to be irreversible due to vulnerability of solvent attack on the redox species,⁶⁰ we observed chemically reversible redox waves in dichloromethane (DCM) and tetrahydrofuran (THF) for oxidation and reduction, respectively. Half-wave potentials of oxidation

and reduction were observed at -2.40 and 0.11 V, respectively, versus the ferrocenium/ferrocene couple (Figure 3). While the

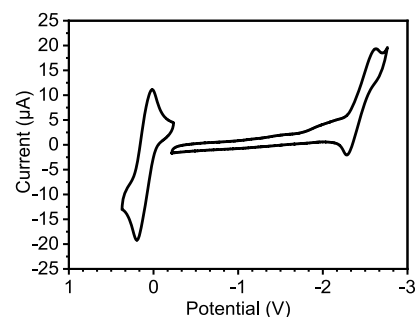


Figure 3. Cyclic voltammograms of Pt(II) complex **8**: quoted against the ferrocenium/ferrocene couple; oxidation: in 1 mM dichloromethane and reduction: 1 mM tetrahydrofuran; electrolyte = 0.1 M tetra-*n*-butylammonium perchlorate; working electrode = glassy carbon; reference electrode = Ag/AgCl; counter electrode = platinum; scan rate = 100 mV/s.

oxidation process can be assigned as the metal oxidation [i.e., Pt(II) \rightarrow Pt(IV)], the reduction can be attributed to ligand reduction with a high proportion of contributions due to the electron-deficient nature of the ligand pyridine ring.⁶¹ Given the reversible redox waves, the energy levels of highest occupied molecular orbital (HOMO) and lowest unoccupied molecular orbital (LUMO) of **8** can be estimated to be -4.9 and -2.4 eV, respectively, using ferrocene with a work function of -4.8 eV from the vacuum level.⁴²

Photophysical Properties. Steady-state photophysical properties of **8** were studied in solution and solid state as shown in Figure 4. The solution absorption and photo-

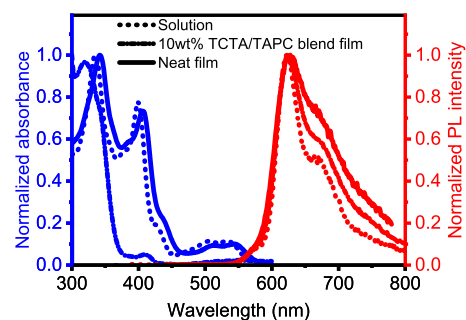


Figure 4. UV–vis absorption and photoluminescence (PL) spectra of **8** in solution (dotted line), blend (dashed line), and neat films (solid line). Solution absorption is in DCM and PL in toluene, while the neat and blend films (10 wt % in TAPC:TCTA = 1:3 by weight) were prepared from freshly distilled DCM solutions and spin-coated at room temperature. Excitation wavelength = 350 nm. Compared solution absorption and PL spectra of **8** in DCM and toluene can be found in Figure S9.

luminescence (PL) spectra of **8** were conducted in DCM and toluene, respectively, while the solid state spectra were obtained from spin-coated neat and blend films [10 wt % in TAPC:TCTA = 1:3, in which TAPC is 1,1-bis[(di-4-tolylamino)phenyl]cyclohexane and TCTA is 4,4',4''-tris(*N*-carbazolyl)triphenylamine], prepared from DCM solutions (15 mg/mL).

The solution absorption spectrum of **8** can be divided into two main regions: a relatively intense high-energy region with

peaks at 335 and 399 nm with molar extinction coefficient, ϵ , $\approx 8800\text{--}6600\text{ dm}^3/(\text{mol cm})$, and a low-intensity, low-energy region ($\approx 410\text{--}560\text{ nm}$ with $\epsilon \approx 1500\text{--}950\text{ dm}^3/(\text{mol cm})$); see the Experimental Section in the [Supporting Information](#) for details. Frontier molecular orbital analysis and TD-DFT data at the B3LYP-D2/SMD/Gen1//B3LYP-D2/Gen1 level of theory were used to characterize these transitions (with solvent = DCM). First, the weak, longer wavelength absorption at $\approx 540\text{ nm}$ can be assigned as the HOMO-to-LUMO transition ([Figure 5](#)). While the LUMO is mainly ligand based, a

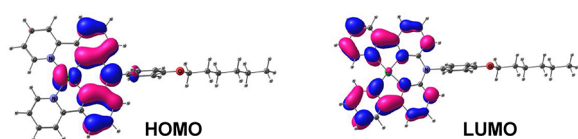


Figure 5. The π -type HOMO of **8** (left), showing significant contribution of metal d_{z^2} and the π^* -like LUMO (right). The absorption observed at 530 nm in the solution phase experiment (calculated value is 528 nm in DCM, [Figure S12a](#)) is due to the HOMO-to-LUMO transition, which accounts for charge transfer from Pt(II) metal and ligand phenyl portion as well as bridge nitrogen to the ligand (both phenyl and pyridyl portions) predominantly.

significant contribution of the metal d-orbital in the HOMO indicates metal-to-ligand charge transfer (MLCT) character in the transition together with ligand center (LC) transitions. The absorption shoulder at $\approx 430\text{ nm}$ corresponds to the HOMO to LUMO+1 transition (i.e., 439 nm; see [Figures S10 and S12a](#)), involving MLCT and LC characters, while the more intense high-energy absorption bands are essentially a result of MLCT transitions (e.g., HOMO–3 to LUMO for peak at 367 nm in [Figures S11 and S12a](#)).

To understand the excited-state dynamics, we further probed these by nanosecond transient absorption spectroscopy by laser flash photolysis in an argon as well as oxygen saturated toluene solution, using a 355 nm nanosecond laser (9 ns) as the excitation source. The transient absorption spectra of **8** ([Figure S13a](#)) exhibited absorption maxima at $\approx 500\text{ nm}$, with a shoulder at $\approx 585\text{ nm}$. The negative change in absorbance or bleach, at approximately 348, 387, and 412 nm, is attributed to the ground-state absorption of **8**, while the negative signal at $\approx 622\text{ nm}$ is due to the PL of **8**. With an increase in spectral time, an overall decrease of absorbance was observed. The transient absorption spectra of **8** in both argon and oxygen atmospheres at 0.24 μs after the laser irradiation are also compared. In the presence of oxygen, the transient signal was completely quenched, suggesting that the transitions ($\approx 410\text{--}550\text{ nm}$) have significant triplet characteristics ([Figure S13a](#)). Transient absorption and emission spectra and steady-state absorption and emission spectra of **8** are shown in [Figure S13b](#) for comparison.

Moving from solution to neat film, all the absorption bands of **8** are red-shifted ([Figure 4](#)). This can be attributed to stronger intermolecular interactions of the complex in the solid state, which is also supported by the TD-DFT calculation results on the dimer units, extracted from the crystal data ([Figure S12](#)).

8 exhibited a deep-red color in a degassed toluene solution with a peak and a shoulder at 627 and $\approx 675\text{ nm}$, respectively. The estimated phosphorescence peak was 674 nm based on the T_1 state geometry ([Figure S15](#)), which is in line with the experimental results (the calculated emission peak was 588 nm

based on the TD-DFT geometry of the S_1 state of **8**, [Figure S14](#)). The compared energy diagram for different states of **8** by using TD-DFT at the B3LYP-D2/SMD/Gen1//B3LYP-D2/Gen1 level is shown in [Figure S16](#). The solution PLQYs and lifetimes for **8** were measured in both DCM and toluene ([Figure S17](#)). The PLQYs were determined against a quinone sulfate reference⁶² with an excitation wavelength of 350 nm. Lifetimes were probed by time-correlated single photon counting (TCSPC). In toluene, the solution PLQY and lifetime were $50 \pm 3\%$ and 5.8 μs , respectively, while in DCM the values were $34 \pm 2\%$ and 5.5 μs , respectively. The microseconds lifetimes indicate the origin of the emission is phosphorescence. In both solvents, the PLQYs of **8** are high for a deep-red phosphorescent Pt(II) complex.

The high solution PLQYs of **8** can be attributed to the rigidity of the complex, restricting rotation of the ligands, in conjunction with the solubilizing surface groups providing the single exponential for the emission lifetime in solution ([Figure S17](#)). This also leads to a narrow PL with a fwhm of $\approx 70\text{ nm}$ ([Figure 4](#)) and low k_{nr} .^{23,26} Moving from solution to solid state, **8** only showed a low neat-film PLQY of $5 \pm 2\%$. Together with broadened neat-film PL spectrum (fwhm $\approx 105\text{ nm}$, [Figure 4](#)), this suggests strong intermolecular interactions of the material, likely resulting from its planar structure. The severe reduction on neat-film PLQY attained in the solid-state spin-coated films indicates ACQ with minimal MMCLT. Nevertheless, the PLQY of the blended films (10 wt % in TAPC:TCTA = 1:3 by weight) increased to $55 \pm 4\%$, in a good agreement with that of dialkylated analogues in Beq₂ (58%, TLEC-025).³³ We also found a biexponential process for the emission lifetime of the blend films ([Figure S17](#) and [Table 1](#)) with much shorter lifetime than that in solution. The

Table 1. Photophysical Properties of **8** in Solution, Spin-Coated Neat Film, and 10 wt % Blend Film in TAPC/TCTA (1:3 by Weight) (from DCM Solution)

| | PLQY (%) | lifetime, τ (μs) | $(\times 10^3\text{ s}^{-1})$ | $(\times 10^3\text{ s}^{-1})$ |
|-----------------------|------------|------------------------------------|-------------------------------|-------------------------------|
| DCM | 34 ± 2 | 5.5 | 0.58 | 1.14 |
| toluene | 50 ± 3 | 5.8 | 0.85 | 0.87 |
| 10 wt % TAPC/ TCTA | 55 ± 4 | 0.3 (9%), 3.8 (91%) | | |
| neat film | 5 ± 2 | | | |

presence of the short-lived component can be attributed to emitting aggregates such as dimers in the blend films even at low doping concentrations (10 wt %).

DFT Calculations of Dimers. To get further insights into the photophysical properties of the emissive dimers in the blend films, DFT calculations were performed, including making use of their crystal packing. The dimer units (**8**···**8**)-a and (**8**···**8**)-b extracted from crystal data were optimized, and monomers with an antiparallel orientation were also considered, creating a third stacked dimer (**8**···**8**)-c.

The B3LYP-D2/Gen1 level optimized monomer geometry of **8** showed excellent agreement with the crystal structures of monomers ([Figure S18](#)). Compared to the Pt···Pt distance of 7.32 Å in the crystal structure, the optimized geometry of (**8**···**8**)-a showed a closer staking of monomers with a Pt···Pt distance of only 3.72 Å ([Figure 6a](#)). The dipoles of the monomers showed an $\approx 120^\circ$ orientation compared to $\approx 90^\circ$ in their crystal structure. Additionally, the optimized geometry of (**8**···**8**)-b nearly reproduces the interdigitating influence of the

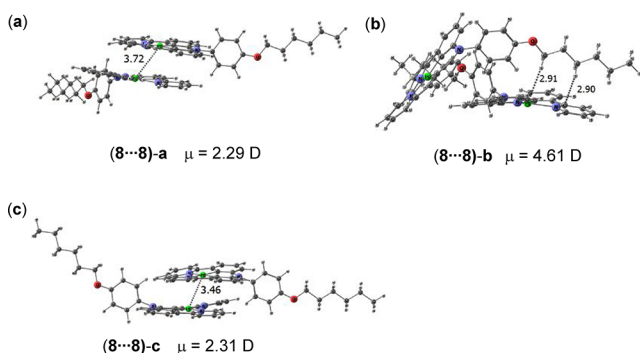


Figure 6. Optimized dimer configurations of **8** by using B3LYP-D2/Gen1 method and the respective dipole moment (μ): (a) stacked dimer, (b) interdigitated dimer, and (c) antiparallely stacked dimer.

hexyloxy tails of one monomer with another (Figure 6b). The third calculated dimer structure (**8**...**8**)-c (which was not observed in crystal structure data) demonstrated a perfect antiparallel stacked orientation between monomers (Figure 6c) with a Pt...Pt distance of 3.46 Å. The calculated interaction energies (E_{int}) for the dimer units (**8**...**8**)-a, (**8**...**8**)-b, and (**8**...**8**)-c were 44.9, 35.6, and 47.1 kcal/mol, respectively. Solvation effect reduces the E_{int} values by 8–10 kcal/mol. In the dimer configuration, monomer dipoles show an antiparallel arrangement with a Pt...Pt distance in the range of 3.46–3.72 Å. This type of association leads to strong orbital interaction between metal centers (Figure S19). In the case of the crystal structure of **8**, a short Pt...Pt distance was not observed, which can be attributed to the formation of (**8**...**8**)-b, as the interdigitating influence of the hexyloxy chains prevents the close association of the coordinating aromatic units. The dimer (**8**...**8**)-b has exhibited the highest dipole moment (μ) 4.61 D while the stacked orientations (**8**...**8**)-a and (**8**...**8**)-c showed μ values of 2.29 and 2.31 D, respectively, which are very close to the

monomer dipole of 2.28 D. The higher transition dipole moment of dimer (**8**...**8**)-b could be the main reason for the biexponential excited-state lifetimes and superior PLQY in a blended film. This is because that transition dipole moment is directly related to oscillator strength. The magnitude of the oscillator strength for an electronic transition is directly proportional to the square of the transition dipole moment produced by the action of electromagnetic radiation on an electric dipole. The oscillator strength qualitatively relates to the strength of the absorption and emission.

OLED Device Properties. With the high blend film PLQYs, OLEDs employing **8** were fabricated with device structure shown in Figure 7a, where the relative energy levels of the materials used can be also found. We used two hole transporting hosts, TAPC and TCTA, to take the advantage of high-lying HOMO of TAPC as well as the high hole mobility of TCTA for reduced turn-on voltage.⁶³ Such blends also offered excellent film forming quality, as can be seen by the absence of any significant structural features in the atomic force microscopy image (Figure S20).

As shown in Figure 7b, the maximum EQE of the OLEDs was recorded to be 6.1% at ≈ 1 cd/m² and reached 4% at 100 cd/m². Figure 7c shows the electroluminescence (EL) at 100 cd/m² with a sharp peak at 623 nm and fwhm of ≈ 55 nm, corresponding to 1931 CIE coordinates of (0.65, 0.35) as saturated red color. The current density–voltage–luminance (J – V – L) characteristics of the OLEDs are shown in Figure 7d, where a low light turn-on voltage (at 1 cd/m²) of 3.3 V was achieved. The maximum brightness of the red OLEDs was 2000 cd/m².

EQE Roll-Off Mechanism. At high current density, EQE roll-off poses a significant issue in phosphorescent OLEDs due to triplet–triplet annihilation, triplet–polaron quenching, and electric field dependent exciton dissociation.^{64–67} To gain insights into these phenomena, small-area OLEDs (0.5 mm²)

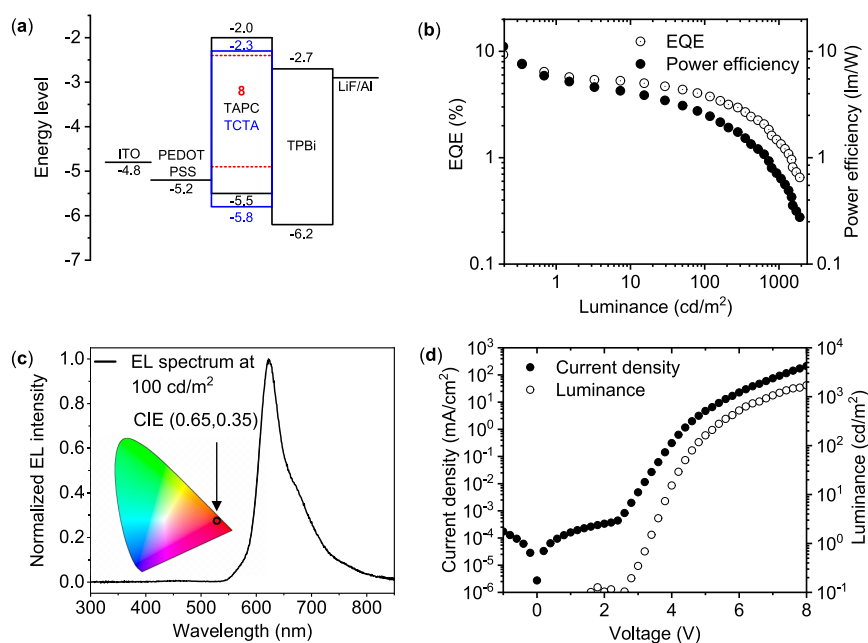


Figure 7. Device performance of deep-red OLEDs. (a) Energy diagrams of materials employed in the devices. (b) External quantum–power efficiency versus luminance plot. (c) EL spectrum at 100 cd/cm² of the diode; inset: CIE coordinates of the deep-red OLED. (d) Current density–luminance versus voltage plots. ITO = indium tin oxide; PEDOT:PSS = poly(3,4-ethylenedioxythiophene)polystyrenesulfonate; TPBi = 1,3,5-tris(*N*-phenylbenzimidazol-2-yl)benzene.

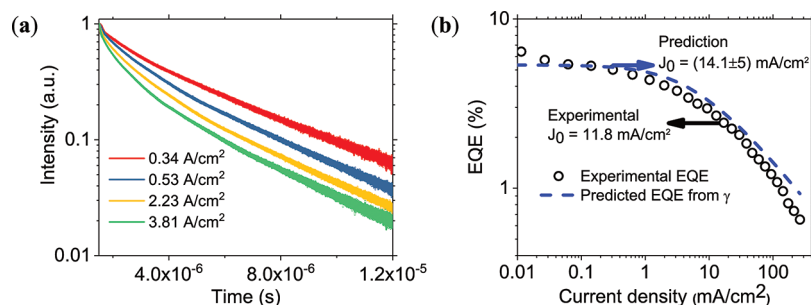


Figure 8. (a) Transient EL decay for different current densities. (b) EQE as a function of current density. The solid line represents the fit using eq 3. The dashed line represents calculated EQE from annihilation model with $\gamma = (1.4 \pm 0.5) \times 10^{-12} \text{ cm}^3/\text{s}$.

were fabricated with the same device structure as those reported in the [Experimental Section](#), and transient EL was measured. Voltage pulses varying between 6 and 12 V were applied to a 0.5 mm² area device at a repetition frequency of 100 Hz to investigate the EL response of the Pt(II)-based OLED. [Figure S21](#) depicts a sample EL response to applied voltage pulse at steady and turn-off states. The 1.5 μs pulses were applied via an AVTECH pulse generator AVX1011-B1-B with a rise and fall time of 2 ns. The EL response was recorded by using a Hamamatsu photomultiplier tube (PMT) (H10721-20) with a response time of 0.57 ns, connected to a Teledyne LeCroy digital oscilloscope (2 GHz) for collecting the optical data.

At higher current density, the EL decay becomes much faster. The faster decay at higher current density is due to the triplet–triplet annihilation process. The annihilation rate constant, γ , can be calculated from the decay of EL intensity ([Figure 8a](#)) via the following equation:^{68,69}

$$\frac{\partial}{\partial t} N(t) = -kN(t) - \gamma N^2(t) \quad (1)$$

where $N(t)$ is the total exciton population and k the exciton decay rate constant. The solution of the equation can be obtained with [eq 2](#):

$$N(t) = \frac{N(0) \exp(-kt)}{1 + \frac{\gamma}{k}[1 - \exp(-kt)]} \quad (2)$$

where $N(0)$ is the initial exciton density. From the fitting of exciton decay plots, we can calculate the annihilation rate constant γ ([Figure S22](#)). The averaged value of γ was determined to be $\approx (1.4 \pm 0.5) \times 10^{-12} \text{ cm}^3/\text{s}$. The value is comparable to those obtained for the Ir(III) dendrimer⁶⁹ and Ir(III) complexes in the TCTA host⁷⁰ by using PL decay at various exciton densities.

The transient annihilation model can be utilized to predict the limiting current density as

$$J_0 = \frac{4qd}{\gamma\tau^2} \quad (3)$$

where J_0 is the onset current density when the EQE drops half of its maximum value, d represents exciton recombination zone thickness, τ is exciton lifetime (phosphorescent lifetime), and q represents the charge of a carrier. Assuming $d = 10 \text{ nm}$ and $\gamma = (1.4 \pm 0.5) \times 10^{-12} \text{ cm}^3/\text{s}$, we estimated $J_0 = 14.1 \pm 5 \text{ mA}/\text{cm}^2$, which is comparable with experimental value of current density when the EQE drops half of its maximum value. Beyond J_0 , the triplet excitons are heavily quenched by

annihilation processes, resulting in a rapid efficiency roll-off in OLED devices.

CONCLUSIONS

In summary, we successfully developed a high-yielding synthetic route to a solution processable highly luminescent Pt(II) complex with a rigid tetradentate structure. The formation of an octahedral Pt(IV) side product is likely responsible for the general poor yields of Pt(II) cyclometalations. By employing a base promoted reduction, we effectively converted the major octahedral Pt(IV) side product into the desired square-planar Pt(II) complex with deep-red emission. The introduction of a hexyloxy solubilizing group enables solution processability of the Pt(II) complex **8**, and high solution and blend film PLQYs ($50 \pm 3\%$ and $55 \pm 4\%$, respectively), despite a small distortion of the square-planar structure. X-ray crystal structures show that while the interdigitation of the hexyloxyphenyl tails attached prevents strong Pt···Pt interaction and minimizes the MMLCT, the perpendicular orientation of molecular dipoles enhances the luminescent properties of Pt(II) complex **8**. OLEDs based on the solution processable **8** exhibited a low turn-on voltage of 3.3 V (at 1 cd/m²) with a maximum EQE of 6.1% (4% at 100 cd/m²) and maximum brightness of 2000 cd/m². Narrow electroluminescence with a peak at 623 nm and a fwhm of $\approx 50 \text{ nm}$ was demonstrated, leading to deep-red emission with 1931 CIE coordinates of (0.65, 0.35).

ASSOCIATED CONTENT

Supporting Information

The Supporting Information is available free of charge on the ACS Publications website at DOI: 10.1021/acsaelm.9b00246.

Materials synthesis and characterization; X-ray crystal structure; thermal properties; photophysical properties; DFT calculations, frontier molecular orbitals and TD-DFT absorption spectrum; nanosecond laser flash photolysis; optical and photophysical characterization; device fabrication/characterization, morphology and device physics; transient EL measurement (PDF)

AUTHOR INFORMATION

Corresponding Authors

*E-mail s.lo@uq.edu.au.

*E-mail e.namdass@uq.edu.au.

ORCID

Ilene Allison: 0000-0002-8499-9872

Hyunsoo Lim: 0000-0002-7636-8923

Kedar Deshmukh: 0000-0002-7981-0932

Robert Wawrzinek: 0000-0002-1186-7625

Sarah K. M. McGregor: 0000-0002-5797-4119

Jack K. Clegg: 0000-0002-7140-5596

Cherumuttathu H. Suresh: 0000-0001-7237-6638

Venugopal Karunakaran: 0000-0001-8482-0900

Narayanan Unni K. N.: 0000-0003-3202-4157

Ayyappanpillai Ajayaghosh: 0000-0001-8574-5391

Ebinazar B. Namdas: 0000-0001-5761-495X

Shih-Chun Lo: 0000-0002-4634-5376

Notes

The authors declare no competing financial interest.

ACKNOWLEDGMENTS

We thank the Australian Research Council (ARC DP140101088 and FT140100273) and Department of Industry, Innovation and Science (AISRF53765) for financial support. We also thank the Department of Science and Technology, Government of India, for financial support (DST/INT/AUS/P-74/2017). I.A., H.L., and V.A. were each funded by an Australian Postgraduate Award and A.S. was funded by UQ's Research and Training Program. This work was performed in part at the Queensland node of the Australian National Fabrication Facility Queensland Node (ANFF-Q)—a company established under the National Collaborative Research Infrastructure Strategy to provide nano- and microfabrication facilities for Australia's researchers. Part of this research was undertaken on the MX1 beamline of the Australian Synchrotron, part of ANSTO. We thank the Australian Synchrotron for travel funding and the beamline staff for their assistance.

REFERENCES

- (1) Kodan, M. *OLED Displays and Lighting*; John Wiley & Sons, Ltd.: 2017.
- (2) Liang, J.; Ying, L.; Huang, F.; Cao, Y. Recent Advances in High Performance Solution Processed WOLEDs for Solid-State Lighting. *J. Mater. Chem. C* **2016**, *4*, 10993–11006.
- (3) Tsujimura, T. OLED Devices. In *OLED Display Fundamentals and Applications*; Sage, A. C. L. I., Ed.; John Wiley & Sons, Inc.: Hoboken, NJ, 2017; pp 36–46.
- (4) Endo, A.; Sato, K.; Yoshimura, K.; Kai, T.; Kawada, A.; Miyazaki, H.; Adachi, C. Efficient Up-Conversion of Triplet Excitons into a Singlet State and its Application for Organic Light Emitting Diodes. *Appl. Phys. Lett.* **2011**, *98*, No. 083302.
- (5) Chou, P. T.; Chi, Y.; Chung, M. W.; Lin, C. C. Harvesting Luminescence via Harnessing the Photophysical Properties of Transition Metal Complexes. *Coord. Chem. Rev.* **2011**, *255*, 2653–2665.
- (6) Fleetham, T.; Li, G. J.; Wen, L. L.; Li, J. Efficient “Pure” Blue OLEDs Employing Tetradentate Pt Complexes with a Narrow Spectral Bandwidth. *Adv. Mater.* **2014**, *26*, 7116–7121.
- (7) Kumar, G. R.; Thilagar, P. Tuning the Phosphorescence and Solid State Luminescence of Triarylborane-Functionalized Acetylacetonato Platinum Complexes. *Inorg. Chem.* **2016**, *55*, 12220–12229.
- (8) Kong, F. K.-W.; Tang, M.-C.; Wong, Y.-C.; Ng, M.; Chan, M.-Y.; Yam, V. W.-W. Strategy for the Realization of Efficient Solution-Processable Phosphorescent Organic Light-Emitting Devices: Design and Synthesis of Bipolar Alkynylplatinum(II) Complexes. *J. Am. Chem. Soc.* **2017**, *139*, 6351–6362.
- (9) Bullock, J. D.; Salehi, A.; Zeman, C. J.; Abboud, K. A.; So, F.; Schanze, K. S. In Search of Deeper Blues: Trans-N-Heterocyclic Carbene Platinum Phenylacetylide as a Dopant for Phosphorescent OLEDs. *ACS Appl. Mater. Interfaces* **2017**, *9*, 41111–41114.

(10) Ma, D.; Tsuboi, T.; Qiu, Y.; Duan, L. Recent Progress in Ionic Iridium(III) Complexes for Organic Electronic Devices. *Adv. Mater.* **2017**, *29*, 1603253.

(11) Zhang, Q.-C.; Xiao, H.; Zhang, X.; Xu, L.-J.; Chen, Z.-N. Luminescent Oligonuclear Metal Complexes and the Use in Organic Light-Emitting Diodes. *Coord. Chem. Rev.* **2019**, *378*, 121–133.

(12) Yook, K. S.; Lee, J. Y. Small Molecule Host Materials for Solution Processed Phosphorescent Organic Light-Emitting Diodes. *Adv. Mater.* **2014**, *26*, 4218–4233.

(13) Nitzan, A.; Mukamel, S.; Jortner, J. Energy Gap Law for Vibrational Relaxation of a Molecule in a Dense Medium. *J. Chem. Phys.* **1975**, *63*, 200–207.

(14) Cummings, S. D.; Eisenberg, R. Tuning the Excited-State Properties of Platinum(II) Diimine Dithiolate Complexes. *J. Am. Chem. Soc.* **1996**, *118*, 1949–1960.

(15) Chan, C.-W.; Cheng, L.-K.; Che, C.-M. Luminescent Donor-Acceptor Platinum(II) Complexes. *Coord. Chem. Rev.* **1994**, *132*, 87–97.

(16) Wilson, J. S.; Chawdhury, N.; Al-Mandhary, M. R. A.; Younus, M.; Khan, M. S.; Raithby, P. R.; Köhler, A.; Friend, R. H. The Energy Gap Law for Triplet States in Pt-Containing Conjugated Polymers and Monomers. *J. Am. Chem. Soc.* **2001**, *123*, 9412–9417.

(17) Huo, S. Q.; Carroll, J.; Vezzu, D. A. K. Design, Synthesis, and Applications of Highly Phosphorescent Cyclometalated Platinum Complexes. *Asian J. Org. Chem.* **2015**, *4*, 1210–1245.

(18) Shen, W.; Zhang, W.; Zhu, C. Theoretical Study of the Substituent Effect Controlling the Radiative and Non-Radiative Decay Processes of Platinum(II) Complexes. *Phys. Chem. Chem. Phys.* **2017**, *19*, 23532–23540.

(19) Boher, P.; Leroux, T.; Collomb-Patton, V.; Bignon, T. Optical Characterization of OLED Displays. *J. Soc. Inf. Dispersion* **2015**, *23*, 429–437.

(20) Giridhar, T.; Han, T. H.; Cho, W.; Saravanan, C.; Lee, T. W.; Jin, S. H. An Easy Route to Red Emitting Homoleptic Ir-III Complex for Highly Efficient Solution-Processed Phosphorescent Organic Light-Emitting Diodes. *Chem. - Eur. J.* **2014**, *20*, 8260–8264.

(21) Cho, W.; Sarada, G.; Maheshwaran, A.; Gal, Y. S.; Nam, Y.; Lee, J. Y.; Jin, S. H. Solution-Processable Highly Efficient Deep-Red and Orange Organic Light-Emitting Diodes Based on Multifunctional Ir(III) Complexes. *J. Mater. Chem. C* **2017**, *5*, 10029–10038.

(22) Liu, X. J.; Yao, B.; Zhang, Z. L.; Zhao, X. F.; Zhang, B. H.; Wong, W. Y.; Cheng, Y. X.; Xie, Z. Y. Power-Efficient Solution-Processed Red Organic Light-Emitting Diodes Based on an Exciplex Host and a Novel Phosphorescent Iridium Complex. *J. Mater. Chem. C* **2016**, *4*, 5787–5794.

(23) Chi, Y.; Tsai, H. Y.; Chen, Y. K. Pt(II) Complexes with Azolate-Containing Bidentate Chelate: Design, Photophysics, and Application. *J. Chin. Chem. Soc.* **2017**, *64*, 574–588.

(24) Yang, X. L.; Yao, C. L.; Zhou, G. J. Highly Efficient Phosphorescent Materials Based on Platinum Complexes and Their Application in Organic Light-Emitting Devices (OLEDs) Platinum complexes Show Promise for Flat Screens and Energy Efficient Lighting. *Platinum Met. Rev.* **2013**, *57*, 2–16.

(25) Wawrzinek, R.; Muhieddine, K.; Ullah, M.; Koszo, P. B.; Shaw, P. E.; Grosjean, A.; Maasoumi, F.; Stoltzfus, D. M.; Clegg, J. K.; Burn, P. L.; Namdas, E. B.; Lo, S.-C. Orange-Red-Light-Emitting Field-Effect Transistors Based on Phosphorescent Pt(II) Complexes with Area Emission. *Adv. Opt. Mater.* **2016**, *4*, 1867–1874.

(26) Li, K.; Ming Tong, G. S.; Wan, Q.; Cheng, G.; Tong, W.-Y.; Ang, W.-H.; Kwong, W.-L.; Che, C.-M. Highly Phosphorescent Platinum(II) Emitters: Photophysics, Materials and Biological Applications. *Chem. Sci.* **2016**, *7*, 1653–1673.

(27) Li, G.; She, Y. Tetradentate Cyclometalated Platinum(II) Complexes for Efficient and Stable Organic Light-Emitting Diodes. In *Light-Emitting Diode - An Outlook On the Empirical Features and Its Recent Technological Advancements*; Thirumalai, J., Ed.; IntechOpen: London, 2018; pp 78–101.

- (28) Fleetham, T.; Li, G. J.; Li, J. Phosphorescent Pt(II) and Pd(II) Complexes for Efficient, High-Color-Quality, and Stable OLEDs. *Adv. Mater.* **2017**, *29*, 1601861.
- (29) Lin, Y. Y.; Chan, S. C.; Chan, M. C. W.; Hou, Y. J.; Zhu, N. Y.; Che, C. M.; Liu, Y.; Wang, Y. Structural, Photophysical, and Electrophosphorescent Properties of Platinum(II) Complexes Supported by Tetradentate N₂O₂ Chelates. *Chem. - Eur. J.* **2003**, *9*, 1263–1272.
- (30) Vezzu, D. A. K.; Deaton, J. C.; Jones, J. S.; Bartolotti, L.; Harris, C. F.; Marchetti, A. P.; Kondakova, M.; Pike, R. D.; Huo, S. Q. Highly Luminescent Tetradentate Bis-Cyclometalated Platinum Complexes: Design, Synthesis, Structure, Photophysics, and Electroluminescence Application. *Inorg. Chem.* **2010**, *49*, 5107–5119.
- (31) Fleetham, T.; Li, G.; Li, J. Efficient Red-Emitting Platinum Complex with Long Operational Stability. *ACS Appl. Mater. Interfaces* **2015**, *7*, 16240–16246.
- (32) Li, G.; Wolfe, A.; Brooks, J.; Zhu, Z.-Q.; Li, J. Modifying Emission Spectral Bandwidth of Phosphorescent Platinum(II) Complexes Through Synthetic Control. *Inorg. Chem.* **2017**, *56*, 8244–8256.
- (33) Fukagawa, H.; Shimizu, T.; Hanashima, H.; Osada, Y.; Suzuki, M.; Fujikake, H. Highly Efficient and Stable Red Phosphorescent Organic Light-Emitting Diodes Using Platinum Complexes. *Adv. Mater.* **2012**, *24*, 5099–5103.
- (34) Kavitha, J.; Chang, S.-Y.; Chi, Y.; Yu, J.-K.; Hu, Y.-H.; Chou, P.-T.; Peng, S.-M.; Lee, G.-H.; Tao, Y.-T.; Chien, C.-H.; Carty, A. J. In Search of High-Performance Platinum(II) Phosphorescent Materials for the Fabrication of Red Electroluminescent Devices. *Adv. Funct. Mater.* **2005**, *15*, 223–229.
- (35) Yang, X.; Jiao, B.; Dang, J.-S.; Sun, Y.; Wu, Y.; Zhou, G.; Wong, W.-Y. Achieving High-Performance Solution-Processed Orange OLEDs with the Phosphorescent Cyclometalated Trinuclear Pt(II) Complex. *ACS Appl. Mater. Interfaces* **2018**, *10*, 10227–10235.
- (36) Yuen, M. Y.; Kui, S. C. E.; Low, K. H.; Kwok, C. C.; Chui, S. S. Y.; Ma, C. W.; Zhu, N. Y.; Che, C. M. Synthesis, Photophysical and Electrophosphorescent Properties of Fluorene-Based Platinum(II) Complexes. *Chem. - Eur. J.* **2010**, *16*, 14131–14141.
- (37) Pander, P.; Bulmer, R.; Martinscroft, R.; Thompson, S.; Lewis, F. W.; Penfold, T. J.; Dias, F. B.; Kozhevnikov, V. N. 1,2,4-Triazines in the Synthesis of Bipyridine Bisphenolate ONNO Ligands and Their Highly Luminescent Tetradentate Pt(II) Complexes for Solution-Processable OLEDs. *Inorg. Chem.* **2018**, *57*, 3825–3832.
- (38) Krikorian, M.; Liu, S.; Swager, T. M. Columnar Liquid Crystallinity and Mechanochromism in Cationic Platinum(II) Complexes. *J. Am. Chem. Soc.* **2014**, *136*, 2952–2955.
- (39) Aliprandi, A.; Mauro, M.; De Cola, L. Controlling and Imaging Biomimetic Self-Assembly. *Nat. Chem.* **2016**, *8*, 10–15.
- (40) Yam, V. W.-W.; Wong, K. M.-C.; Zhu, N. Solvent-Induced Aggregation through Metal···Metal/ π ··· π Interactions: Large Solvatochromism of Luminescent Organoplatinum(II) Terpyridyl Complexes. *J. Am. Chem. Soc.* **2002**, *124*, 6506–6507.
- (41) Kim, K. H.; Liao, J. L.; Lee, S. W.; Sim, B.; Moon, C. K.; Lee, G. H.; Kim, H. J.; Chi, Y.; Kim, J. J. Crystal Organic Light-Emitting Diodes with Perfectly Oriented Non-Doped Pt-Based Emitting Layer. *Adv. Mater.* **2016**, *28*, 2526–2532.
- (42) Lo, S.-C.; Harding, R. E.; Shipley, C. P.; Stevenson, S. G.; Burn, P. L.; Samuel, I. D. W. High-Triplet-Energy Dendrons: Enhancing the Luminescence of Deep Blue Phosphorescent Iridium(III) Complexes. *J. Am. Chem. Soc.* **2009**, *131*, 16681–16688.
- (43) Mai, V. T. N.; Shukla, A.; Mamada, M.; Maedera, S.; Shaw, P. E.; Sibus, J.; Allison, I.; Adachi, C.; Namdas, E. B.; Lo, S.-C. Low Amplified Spontaneous Emission Threshold and Efficient Electroluminescence from a Carbazole Derivatized Excited-State Intramolecular Proton Transfer Dye. *ACS Photonics* **2018**, *5*, 4447–4455.
- (44) Chassot, L.; Von Zelewsky, A.; Sandrini, D.; Maestri, M.; Balzani, V. Photochemical Preparation of Luminescent Platinum(IV) Complexes via Oxidative Addition on Luminescent Platinum(II) Complexes. *J. Am. Chem. Soc.* **1986**, *108*, 6084–6085.
- (45) Juliá, F.; García-Legaz, M.-D.; Bautista, D.; González-Herrero, P. Influence of Ancillary Ligands and Isomerism on the Luminescence of Bis-Cyclometalated Platinum(IV) Complexes. *Inorg. Chem.* **2016**, *55*, 7647–7660.
- (46) Hill, R. H.; Puddephatt, R. J. A Mechanistic Study of the Photochemically Initiated Oxidative Addition of Isopropyl Iodide to Dimethyl(1,10-phenanthroline)platinum(II). *J. Am. Chem. Soc.* **1985**, *107*, 1218–1225.
- (47) Whitfield, S. R.; Sanford, M. S. Reactions of Platinum(II) Complexes with Chloride-Based Oxidants: Routes to Pt(III) and Pt(IV) Products. *Organometallics* **2008**, *27*, 1683–1689.
- (48) Mamtora, J.; Crosby, S. H.; Newman, C. P.; Clarkson, G. J.; Rourke, J. P. Platinum(IV) Complexes: C–H Activation at Low Temperatures. *Organometallics* **2008**, *27*, 5559–5565.
- (49) Jenkins, D. M.; Bernhard, S. Synthesis and Characterization of Luminescent Bis-Cyclometalated Platinum^{IV} Complexes. *Inorg. Chem.* **2010**, *49*, 11297–11308.
- (50) Juliá, F.; Bautista, D.; Fernández-Hernández, J. M.; González-Herrero, P. Homoleptic Tris-Cyclometalated Platinum(IV) Complexes: A New Class of Long-Lived, Highly Efficient ³LC Emitters. *Chem. Sci.* **2014**, *5*, 1875–1880.
- (51) Newman, C. P.; Casey-Green, K.; Clarkson, G. J.; Cave, G. W. V.; Errington, W.; Rourke, J. P. Cyclometalated Platinum(II) Complexes: Oxidation to, and C–H Activation by, Platinum(IV). *Dalton Trans.* **2007**, 3170–3182.
- (52) Parker, R. R.; Sarju, J. P.; Whitwood, A. C.; Williams, J. A. G.; Lynam, J. M.; Bruce, D. W. Synthesis, Mesomorphism, and Photophysics of 2,5-Bis(dodecyloxyphenyl)pyridine Complexes of Platinum(IV). *Chem. - Eur. J.* **2018**, *24*, 19010–19023.
- (53) Zhang, Y.; Meng, F.; You, C.; Yang, S.; Xiong, L.; Xiong, W.; Zhu, W.; Wang, Y.; Pei, Y.; Su, S. Efficient Near-Infrared Emitting Tetradentate Bis-Cyclometalated Platinum(IV) Complexes for Solution-Processed Polymer Light-Emitting Diodes. *Dyes Pigm.* **2017**, *142*, 457–464.
- (54) Hang, X.-C.; Fleetham, T.; Turner, E.; Brooks, J.; Li, J. Highly Efficient Blue-Emitting Cyclometalated Platinum(II) Complexes by Judicious Molecular Design. *Angew. Chem., Int. Ed.* **2013**, *52*, 6753–6756.
- (55) Li, G.; Klimes, K.; Fleetham, T.; Zhu, Z.-Q.; Li, J. Stable and Efficient Sky-Blue Organic Light Emitting Diodes Employing a Tetradentate Platinum Complex. *Appl. Phys. Lett.* **2017**, *110*, 113301.
- (56) Liu, G.; Liang, F.; Zhao, Y.; Hu, H.; Fan, J.; Liao, L.-S. Phosphorescent Platinum(II) Complexes Based on Spiro Linkage-Containing Ligands. *J. Mater. Chem. C* **2017**, *5*, 1944–1951.
- (57) Zhang, X.-Q.; Xie, Y.-M.; Zheng, Y.; Liang, F.; Wang, B.; Fan, J.; Liao, L.-S. Highly Phosphorescent Platinum(II) Complexes Based on Rigid Unsymmetric Tetradentate Ligands. *Org. Electron.* **2016**, *32*, 120–125.
- (58) Zhu, Z.-Q.; Klimes, K.; Holloway, S.; Li, J. Efficient Cyclometalated Platinum(II) Complex with Superior Operational Stability. *Adv. Mater.* **2017**, *29*, 1605002.
- (59) Johnson, R. C.; Basolo, F. Substitution Reactions of Platinum(IV) Complexes: The Synthesis and Properties of Trans-Dithiocyanato-Bis-(Ethylenediamine)Platinum(IV) Salts. *J. Inorg. Nucl. Chem.* **1960**, *13*, 36–43.
- (60) Kvam, P.-I.; Puzyk, M. V.; Balashev, K. P.; Songstad, J.; Lundberg, C.; Arnarp, J.; Bjork, L.; Gawinecki, R. Spectroscopic and Electrochemical Properties of Some Mixed-Ligand Cyclometalated Platinum(II) Complexes Derived from 2-Phenylpyridine. *Acta Chem. Scand.* **1995**, *49*, 335–343.
- (61) Brooks, J.; Babayan, Y.; Lamansky, S.; Djurovich, P. I.; Tsyba, I.; Bau, R.; Thompson, M. E. Synthesis and Characterization of Phosphorescent Cyclometalated Platinum Complexes. *Inorg. Chem.* **2002**, *41*, 3055–3066.
- (62) Crosby, G. A.; Demas, J. N. Measurement of Photoluminescence Quantum Yields. A Review. *J. Phys. Chem.* **1971**, *75*, 991–1024.
- (63) Fu, Q.; Chen, J. S.; Shi, C. S.; Ma, D. G. Solution-Processed Small Molecules as Mixed Host for Highly Efficient Blue and White

Phosphorescent Organic Light-Emitting Diodes. *ACS Appl. Mater. Interfaces* **2012**, *4*, 6579–6586.

(64) Reineke, S.; Walzer, K.; Leo, K. Triplet-Exciton Quenching in Organic Phosphorescent Light-Emitting Diodes with Ir-Based Emitters. *Phys. Rev. B: Condens. Matter Mater. Phys.* **2007**, *75*, 125328.

(65) Baldo, M. A.; Adachi, C.; Forrest, S. R. Transient Analysis of Organic Electrophosphorescence. II. Transient Analysis of Triplet-Triplet Annihilation. *Phys. Rev. B: Condens. Matter Mater. Phys.* **2000**, *62*, 10967–10977.

(66) Song, D. D.; Zhao, S. L.; Luo, Y. C.; Aziz, H. Causes of Efficiency Roll-Off in Phosphorescent Organic Light Emitting Devices: Triplet-Triplet Annihilation Versus Triplet-Polaron Quenching. *Appl. Phys. Lett.* **2010**, *97*, 243304.

(67) Kalinowski, J.; Stampor, W.; Mezyk, J.; Cocchi, M.; Virgili, D.; Fattori, V.; Di Marco, P. Quenching Effects in Organic Electrophosphorescence. *Phys. Rev. B: Condens. Matter Mater. Phys.* **2002**, *66*, 235321.

(68) Shaw, P. E.; Ruseckas, A.; Samuel, I. D. W. Exciton Diffusion Measurements in Poly(3-hexylthiophene). *Adv. Mater.* **2008**, *20*, 3516–3520.

(69) Namdas, E. B.; Ruseckas, A.; Samuel, I. D. W.; Lo, S.-C.; Burn, P. L. Triplet Exciton Diffusion in *fac*-Tris(2-Phenylpyridine)Iridium(III)-Cored Electroluminescent Dendrimers. *Appl. Phys. Lett.* **2005**, *86*, No. 091104.

(70) Ligthart, A.; de Vries, X.; Zhang, L.; Pols, M. C. W. M.; Bobbert, P. A.; van Eersel, H.; Coehoorn, R. Effect of Triplet Confinement on Triplet-Triplet Annihilation in Organic Phosphorescent Host-Guest Systems. *Adv. Funct. Mater.* **2018**, *28*, 1804618.